



Establishment and application of a zebrafish model of Werner syndrome identifies sapanisertib as a potential antiaging drug

Jianlong Ma^{a,1} , Yang Chen^{b,1}, Jingmei Song^b, Qingfeng Ruan^b, Lianghui Li^b, and Lingfei Luo^{a,b,2}

Affiliations are included on p. 11.

Edited by Duoja Pan, The University of Texas Southwestern Medical Center, Dallas, TX; received July 9, 2024; accepted January 3, 2025

Aging is a complex process that affects multiple organs, and the discovery of a pharmacological approach to ameliorate aging is considered the Holy Grail of medicine. Here, we performed an N-ethyl-N-nitrosourea forward genetic screening in zebrafish and identified an accelerated aging mutant named *meteor* (*met*), harboring a mutation in the *Werner syndrome RecQ-like helicase* (*wrn*) gene. Loss of *wrn* leads to a short lifespan and age-related characteristics in the intestine of zebrafish embryos, such as cellular senescence, genomic instability, and epigenetic alteration. Therefore, we conducted a screening of antiaging drugs using the *met* mutant and revealed that sapanisertib effectively ameliorated most of the aging phenotypes of the mutant. Mechanistically, the geroprotective effects of sapanisertib may be attributed to inhibition of mTORC1/2. Furthermore, sapanisertib also attenuated chronological aging in wild-type aged zebrafish and replicative-senescence in human foreskin fibroblasts. Taken together, our study introduces a unique and efficient model for large-scale antiaging drug screening in vertebrates and suggests sapanisertib as a potential therapeutic option for treating premature aging and promoting healthy aging.

wrn | drug screening | premature aging | mTORC1/2 signaling

Aging is characterized by a gradual decline of physical and psychological functions that affects individuals worldwide (1, 2). In recent years, the study of aging has become a key focus for researchers (3). Classical invertebrate models, such as *Caenorhabditis elegans* and fruit flies, have played a pivotal role in identifying conserved genes and signaling pathways that regulate aging and extend lifespan due to their short lifespans, well-defined genetic backgrounds, and ease of manipulation (4, 5). However, these invertebrate models lack key organs and systems that are crucial in human aging, such as blood and an adaptive immune system, making it difficult to fully recapitulate human aging processes (6). Consequently, vertebrate models, such as mice and zebrafish, have become essential tools for aging research. For example, studies in rodents have shown that caloric restriction extends lifespan (7), while zebrafish have played a crucial role in studying functional aging and modeling age-related diseases (8).

With the aging population on the rise, there is an urgent need to discover geroprotective drugs that attenuate aging and alleviate aging-related diseases (9). Due to the generally long lifespans of vertebrates, various premature aging models in mice and zebrafish have been established, providing valuable tools for identifying antiaging drugs (3, 10, 11). For instance, the effects of farnesyltransferase inhibitor on ameliorating premature aging were assessed using the *Zmpste24^{-/-}* progeria mice model (12). Similarly, a study on the zebrafish *rag1^{-/-}* model has shown that senolytic drugs and antioxidants significantly reduce the accumulation of senescent cells (13). Moreover, the turquoise killifish, with a natural lifespan of only 4 to 6 mo, has become an important vertebrate model for studying aging (14). Recent studies demonstrated that a dasatinib–quercetin combination exhibited neuroprotective effects in the killifish model, alleviating age-associated functional decline (15). Additionally, the Interventions Testing Program (ITP) has systematically evaluated several potential antiaging compounds, confirming the antiaging effects of drugs such as rapamycin, resveratrol, and acarbose (16, 17). Although short-lived vertebrate models and the ITP have made significant contributions to validating antiaging drugs, their capacity for high-throughput compound screening is limited. As a result, the screening of antiaging drugs has mainly been limited to in vitro or invertebrate species (18, 19). Consequently, developing a vertebrate model suitable for high-throughput screening of antiaging compounds is crucial for identifying potential geroprotective drugs.

The zebrafish contains orthologs of 71% of human genes and 82% of disease-causing human proteins, making it a powerful preclinical vertebrate model for human disease (20–23). In addition, with the advantages of high fecundity, small size, and cost-effectiveness, zebrafish is now established as the representative vertebrate model for high-throughput and

Significance

With the rapid aging of the world population, it is crucial to identify geroprotective drugs that attenuate age-related health decline. Due to the long lifespan of vertebrates, antiaging drug screening has mostly been limited to in vitro or invertebrate models, which poorly mimic human aging. Thus, developing short-lived vertebrate models with accelerated aging is essential for efficient and large-scale drug screening. Herein, we established a zebrafish model exhibiting premature aging features. Using this model for high-throughput drug screening, we identified sapanisertib as a promising antiaging compound. Additionally, sapanisertib attenuated chronological aging in aged zebrafish and replicative senescence in human foreskin fibroblasts (HFF), supporting its potential as a unique therapeutic option for treating premature aging and promoting healthy aging.

Author contributions: J.M., Y.C., and L. Luo designed research; J.M., Y.C., J.S., Q.R., and L. Li performed research; J.M. and Y.C. analyzed data; and J.M., Y.C., and L. Luo wrote the paper.

Competing interest statement: The authors declare that they have patent application filings to disclose (2024112106528).

This article is a PNAS Direct Submission.

Copyright © 2025 the Author(s). Published by PNAS. This article is distributed under Creative Commons Attribution-NonCommercial-NoDerivatives License 4.0 (CC BY-NC-ND).

¹J.M. and Y.C. contributed equally to this work.

²To whom correspondence may be addressed. Email: lluo@fudan.edu.cn.

This article contains supporting information online at <https://www.pnas.org/lookup/suppl/doi:10.1073/pnas.2413719122/-DCSupplemental>.

Published January 30, 2025.

high-content phenotypic drug screening (24, 25). Consequently, obtaining zebrafish mutants that exhibit premature aging at the embryonic stage would enable large-scale drug screening in vertebrates. Here, we identified a zebrafish mutant, named *met*, that displayed a premature aging phenotype through an N-ethyl-N-nitrosourea (ENU) forward genetic screening. The aging phenotype in the *met* mutant results from a mutation in *wrn*, a gene in the conserved RecQ helicase family. In humans, mutations in the *WRN* gene result in Werner syndrome (WS), a rare autosomal-recessive genetic disorder characterized by features of accelerated aging (26, 27). A previous study reported that zebrafish *wrn* mutants exhibit a shortened body size and revealed the role of *wrn* in bone development, but typical premature aging symptoms have not been observed (28). Additionally, mutation in *blm*, another member of the RecQ helicase family, has been shown to disrupt germline development without leading to premature aging phenotypes (29).

In contrast, our *met* mutant recapitulates age-related features of WS in the intestine at 8 days postfertilization (dpf). The small size of 8 dpf zebrafish embryos allows them to be easily placed in a 24-well plate, enabling high-throughput drug screening with minimal compound usage. This makes the *met* mutant an ideal model for large-scale antiaging drug screening, providing a rapid, cost-efficient, and high-throughput platform for investigating potential treatments for WS and aging-related diseases. Following a high-throughput antiaging drug screening using the *met* mutant,

we identified sapanisertib as a geroprotective agent against both premature and chronological aging.

Results

The *met* Mutant Exhibits Cellular Senescence in the Intestine of Zebrafish Larvae.

To identify different accelerated aging mutants in zebrafish, we performed an ENU mutagenesis and forward genetic screening. As the senescence-associated β -galactosidase (SA- β -Gal) activity is considered one of the most widely recognized markers of cellular senescence (30), the zebrafish larvae were fixed at 8 dpf for subsequent assessment of cellular senescence using SA- β -Gal assay. A recessive mutant named *met*, characterized by cellular senescence in the intestine marked by SA- β -Gal, but without apparent body defects, was identified (Fig. 1A and B). The intestine is suggested to be one of the earliest organs to exhibit signs of aging, with hallmarks of aging first observed in the intestine, supporting its role as an indicator of systemic aging (31–33), thus suggesting that *met* mutants develop a premature aging phenotype.

The Senescence Phenotype in the *met* Mutant Is Caused by Mutation of the *wrn* Gene.

To isolate the gene disrupted in the *met* mutant, we used a standard set of simple sequence length polymorphism (SSLP) markers and located the mutation site on chromosome 10. After fine mapping and genomic sequencing

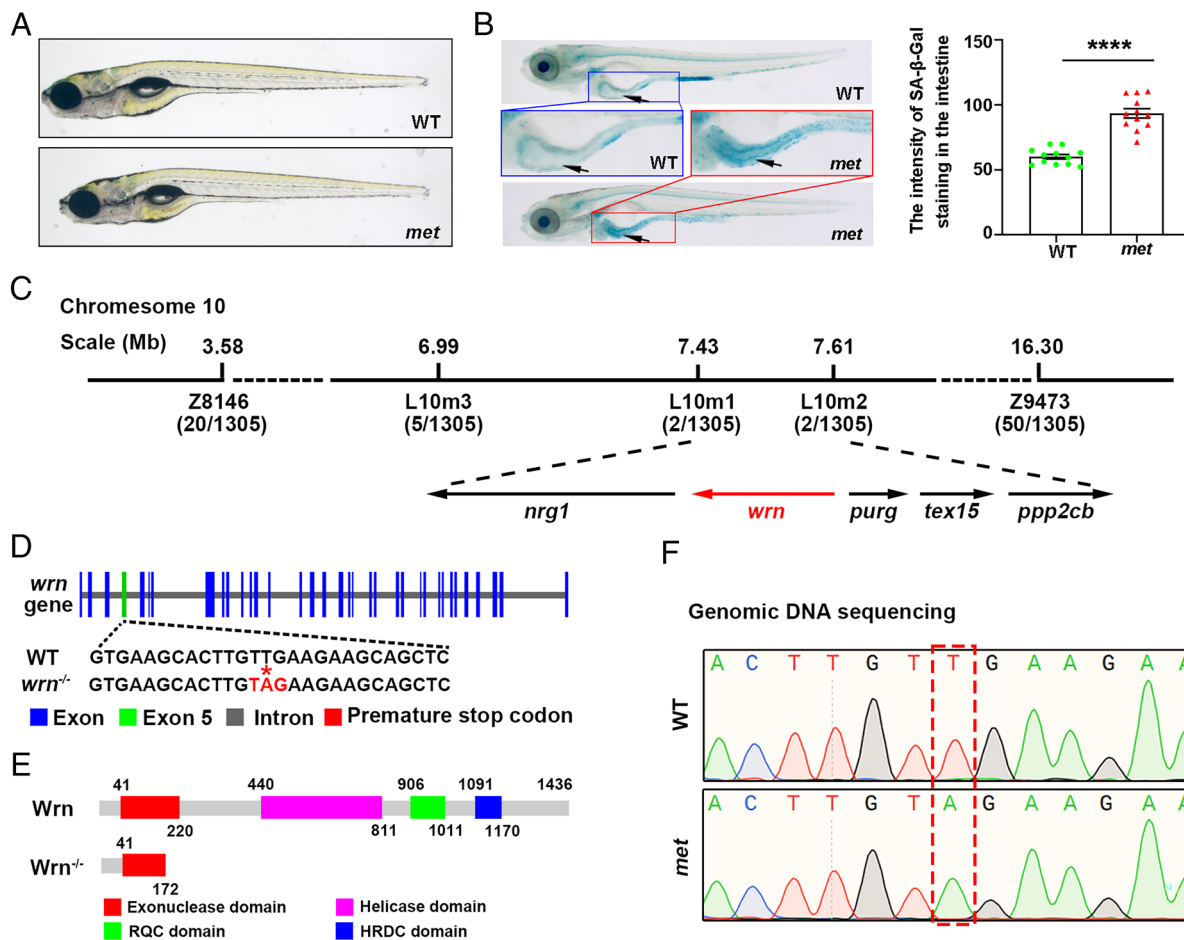


Fig. 1. The *met* mutant with *wrn* gene mutation exhibits cellular senescence. (A) Bright-field images showing the morphological appearance of WT and *met* mutants at 8 dpf. (B) Representative image of SA- β -Gal staining and quantification of the intensity of SA- β -Gal staining in the intestine at 8 dpf ($n = 12$ for each group). Arrows indicate the intestine region. (C) Genetic map of the candidate region on chromosome 10. Numbers below SSLP indicate recombination events. (D) Diagram showing the genomic structure of *wrn* between WT and *met*. (E) Schematic representation of the change in function domains of Wrn between WT and *met*. (F) The genomic sequencing results displaying the mutation site in *wrn*. Note that the T to A transition (red dashed box) leading a premature stop codon within the coding region in the *met* mutant. Data are presented as mean \pm SEM. Significance was determined by the unpaired *t* test. **** $P < 0.0001$. BF, bright-field; dpf, day postfertilization; WT, wild type; SSLP, simple sequence length polymorphism.

of the candidate genes, we located the *met* mutation site to *wrn* genomic loci (Fig. 1C). Sequencing results showed that the *met* mutant allele bears a T to A transition in the 50th bp of exon 5 of the *wrn* gene, leading to a premature stop codon and truncated protein product of only 172 amino acids instead of the 1,436 amino acids of the full-length protein (Fig. 1 D–F).

To confirm whether the *wrn* mutation was responsible for the aging phenotype in the *met* mutant, we generated a *wrn* mutant line *wrn*^{KO} using CRISPR/Cas9 technology. Due to the ENU nonsense mutation resulting in loss of 88% of the Wrn protein, we designed two specific gRNAs targeting exon 4 and exon 35 of *wrn*, respectively, for large fragment deletion to mimic the truncated protein caused by the ENU mutation (*SI Appendix*, Fig. S1A). Gel electrophoresis and sequencing result indicated that the 87% of coding sequence of *wrn*, and 57.8% of the exonuclease domain was deleted in the *wrn*^{KO} mutant (*SI Appendix*, Fig. S1B–D). The *wrn*^{KO} mutant larvae showed normal body shape, but exhibited cellular senescence in the intestine, consistent with the phenotype of the *met* mutant (*SI Appendix*, Fig. S2 A and B). To further validate that the aging phenotype was caused by *wrn* mutation, we performed a heat shock-induced rescue experiment using *Tg(hsp70l:wrn-HA-p2A-mCherry)*, in which *wrn* will be overexpressed after heat-shock induction (*SI Appendix*, Fig. S3A). Cellular senescence in the *met* mutant could be rescued by *wrn* overexpression, as identified by the red fluorescence of mCherry (*SI Appendix*, Fig. S3 B and C). These results demonstrate that the phenotype of cellular senescence in the *met* mutant is caused by *wrn* mutation.

The Zebrafish *wrn*^{KO} Mutants Recapitulate the Age-Related Characteristics of WS Patients. *WRN* mutations were linked to WS, which is characterized by accelerated aging in humans, making it an ideal model for aging research (34). However, *Wrn*^{−/−} mice failed to recapitulate the phenotypes of WS patients (35–37), resulting in a lack of vertebrate animal models for studying WS. Therefore, we examined whether the *wrn*^{KO} zebrafish mutant exhibits the features of accelerated aging similar to human WS. Besides SA-β-Gal staining, increased expression levels of *p21* and *p53* (38), hallmarks of cellular senescence, in the intestine of *wrn*^{KO} mutants also indicate cellular senescence (Fig. 2A). Given that *p53* protein is primarily regulated by protein degradation via the Mdm2–proteasome axis (39), we further analyzed *p53* expression using Western blotting, and the results were consistent with those from qPCR (Fig. 2B). In addition, *wrn*^{KO} mutants showed short lifespan, another distinct feature of WS patients (Fig. 2C). Moreover, studies have shown that WS patients have a higher risk of developing fatty liver (40). The whole-mount oil red O (ORO) lipid staining assay and the whole-mount *in situ* hybridization (WISH) results of the fatty liver marker *cetp* showed a considerable lipid accumulation in the liver of the *wrn*^{KO} mutant (Fig. 2D). In addition, a common congenital symptom of WS is short stature (41). Accordingly, we measured the body length of *wrn*^{KO} mutants and wild-type (WT). Although embryonic development was unaffected by *wrn* mutation, the body size of *wrn*^{KO} mutants was decreased significantly compared with WT from around 15 dpf (Fig. 2E). Accumulation of DNA damage, a driving force of aging and age-related pathology, is also regarded as one of the primary causes of WS (42, 43). To assess the level of endogenous DNA damage in the *wrn*^{KO} mutant, we quantified the typical DNA damage marker, phosphorylated H2AX (γH2AX). Meanwhile, we employed the transgenic line *Tg(fabp2:Dendra2-NTR)*, in which the intestine epithelial cells were labeled by Dendra2, to indicate the intestine (44). γH2AX was scarcely observed in WT, however, *wrn*^{KO} mutants showed a

significant increase and accumulation of γH2AX positive cells in the intestine at 8 dpf (Fig. 2F). Another characteristic of premature cellular aging in WS patients is altered epigenetic marks, including global loss of H3K9me3 (45). Antibody staining showed that the expression of H3K9me3 was robust in the WT, whereas it was significantly weakened in the intestine of *wrn*^{KO} mutants (Fig. 2G).

To ensure that the aging phenotypes observed in *met* mutants were not influenced by potential second-site mutations from the ENU mutagenesis, we performed comparative analyses between the *met* mutants and CRISPR/Cas9-generated *wrn*^{KO} zebrafish. Both *wrn*^{KO} and *met* mutants exhibited consistent aging-associated phenotypes, including increased DNA damage, decreased H3K9me3 levels, and increased expression of senescence markers *p21* and *p53* in the intestine, and short body length at later stages (*SI Appendix*, Fig. S2 C–J). Hepatic lipid accumulation, as assessed by ORO staining and *cetp* expression, was also comparable in both mutants (*SI Appendix*, Fig. S2K). No significant differences were observed between the *met* and *wrn*^{KO} mutants in any of the phenotypic assessments.

Besides, we also performed a heat shock-induced rescue experiment using *Tg(hsp70l:wrn-HA-p2A-mCherry)* to overexpress *wrn* in *met* mutants and assess whether other aging phenotypes could be rescued. The overexpression of *wrn* significantly reversed the aging phenotypes, including reducing γH2AX-positive cells, restoring H3K9me3 expression, normalizing *p21* and *p53* levels, alleviating hepatic lipid accumulation, and ameliorating the short body length at 30 and 45 dpf (*SI Appendix*, Fig. S3 D–J). Similarly, *wrn* overexpression in *wrn*^{KO} zebrafish also rescued the increased DNA damage phenotype, as evidenced by reduced γH2AX staining (*SI Appendix*, Fig. S4 A and B). Together, these findings collectively demonstrate that the aging phenotypes in both *met* and *wrn*^{KO} mutants are specifically caused by the *wrn* mutation.

Since *p53* levels are significantly up-regulated in *wrn*^{KO} mutants, we introduced the *tp53*^{M214K} mutant (*p53*^{−/−}) into the *wrn*^{KO} mutant, which abrogated normal *p53* function (46). Our findings show that *p53* deficiency does not rescue the aging phenotypes of *wrn*^{KO} mutants (*SI Appendix*, Fig. S5), suggesting that the observed phenotypes in the *wrn*^{KO} mutants are independent on *p53* activity. Overall, our findings suggest that the zebrafish *wrn*^{KO} mutant serves as a valuable vertebrate animal model for studying WS.

Since WS is a progeroid syndrome closely resembling natural aging (27), we further assessed whether zebrafish *wrn*^{KO} mutants exhibit chronological aging markers. As intestine permeability has been highlighted as a key phenotype of aging (47, 48), we examined whether *wrn*^{KO} mutants exhibit defects in intestinal barrier function. After feeding zebrafish with fluorescent dextran (FITC-dextran), WT larvae retained dextran in the intestinal lumen, whereas in *wrn*^{KO} mutants, dextran breached the intestinal epithelium and diffused into the circulatory system, indicating compromised intestinal barrier function in the mutants (*SI Appendix*, Fig. S6A). Given the strong association between severe intestinal barrier dysfunction and premature death (47, 48), this may partially explain the premature mortality observed in *wrn*^{KO} mutants, which occurs before the stage of sexual maturity. Additionally, inflammation, a hallmark of chronological aging, was analyzed (2, 49). Transcriptional profile analyses revealed upregulation of inflammation-related genes in the intestine of mutants (*SI Appendix*, Fig. S6B), which was subsequently validated by qPCR, showing increased expression of *lect2l*, *il1b*, *cxcl18a*, *mpx*, and *mmp9* in *wrn*^{KO} mutants (*SI Appendix*, Fig. S6C). Furthermore, ER stress, a feature associated with aging in some human tissues (48), was assessed. The *hspa5* and *xbp-1*, key regulatory genes of ER stress, were found to be significantly up-regulated in the intestine of *wrn*^{KO} mutants, as demonstrated

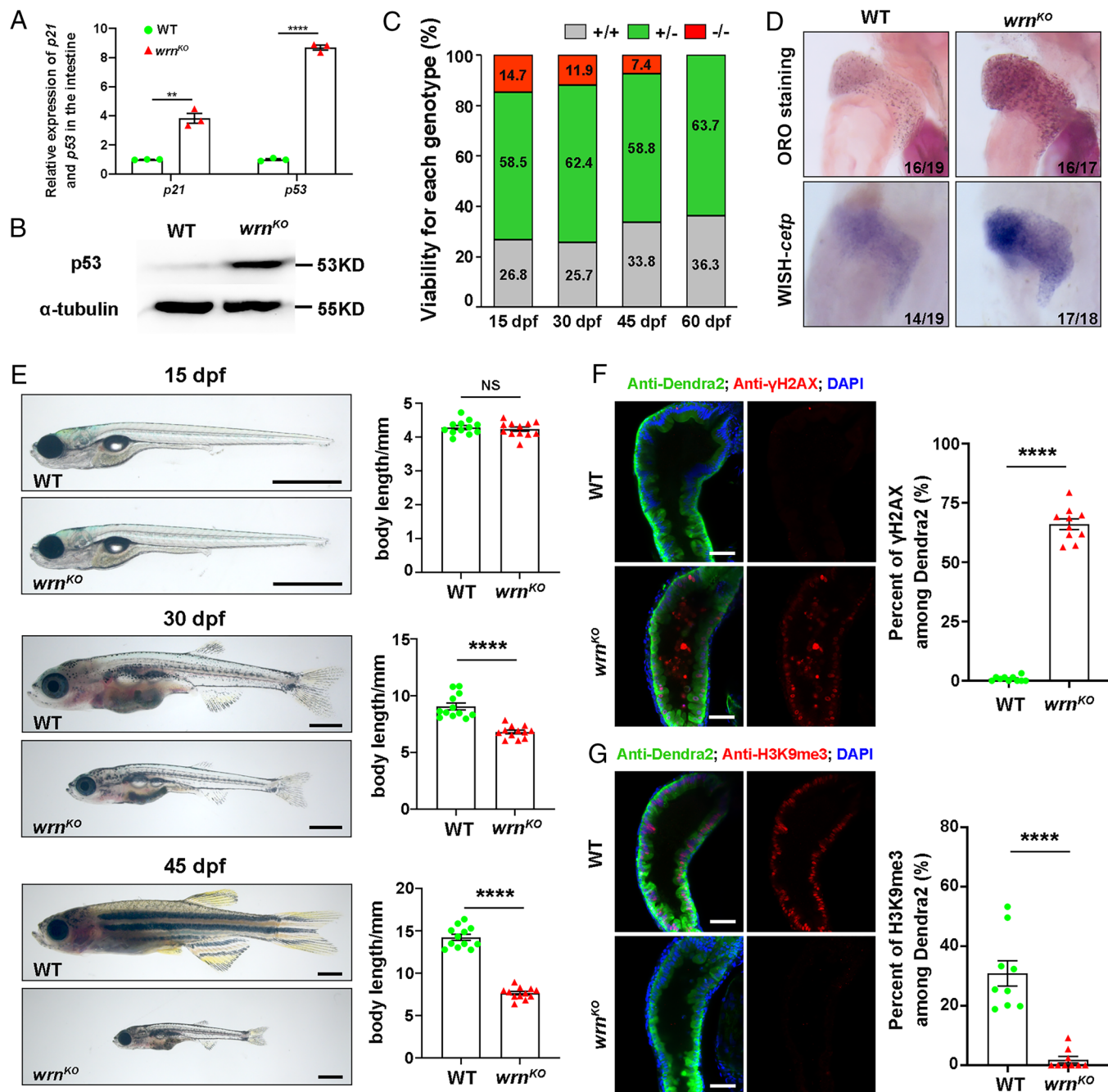


Fig. 2. The zebrafish *wrn*^{KO} mutants recapitulate the age-related characteristics of WS patients. (A) qPCR analysis of age-related gene expression (*p21* and *p53*) in intestinal samples at 8 dpf ($n = 40$ for each group). (B) Western blot images of *p53* in WT and *wrn*^{KO} mutant larvae in intestinal samples at 8 dpf ($n = 40$ for each group). (C) Viability for WT and *wrn*^{KO} at 15 dpf, 30 dpf, 45 dpf, and 60 dpf. (D) ORO staining (Top) and WISH of *cetp* (Bottom) at 8 dpf in WT and *wrn*^{KO} mutants. Numbers indicate the proportion of larvae exhibiting the expression shown. (E) Representative phenotypic images of WT and *wrn*^{KO} mutants at the specified time points (15 dpf, 30 dpf, and 45 dpf) and quantification of the body length ($n = 12$ for each group). (F) Single-optical section images showing the expression of γ H2AX (red), Dendra2 (green), and DAPI (blue) in the intestine of *Tg(fabp2:Dendra2-NTR)* between WT and *wrn*^{KO} mutants at 8 dpf. Quantification of the percent of γ H2AX ($n = 10$ for each group). (G) Single-optical section images showing the expression of H3K9me3 (red), Dendra2 (green), and DAPI (blue) in the intestine of *Tg(fabp2:Dendra2-NTR)* between WT and *wrn*^{KO} mutants at 8 dpf. Quantification of the percent of H3K9me3 ($n = 9$ for each group). [Scale bars, 1 mm (E) and 50 μ m (F and G).] Data are presented as mean \pm SEM. Significance was determined by the unpaired *t* test. NS, not significant; ** $P < 0.01$; *** $P < 0.0001$. ORO, whole-mount Oil Red O; WISH, whole-mount in situ hybridization.

by WISH analysis (SI Appendix, Fig. S6D). Together, these findings suggest that *wrn*^{KO} mutants recapitulate several chronological aging features, supporting their validity as a model for studying aging mechanisms.

Drug Screening Identifies Sapanisertib as Ameliorating Aging Phenotypes in *wrn*^{KO} Mutants. The relatively long lifespan of vertebrates poses an apparent obstacle for performing large-scale screening of antiaging drugs. Here, we observed that the zebrafish

wrn^{KO} mutant exhibit accelerated senescence within 8 d, offering the potential for high-throughput geroprotective drug screening in vertebrates. Therefore, we conducted an antiaging drug screening on the zebrafish *wrn*^{KO} mutant using the SA- β -Gal assay, a widely accepted measure of cellular senescence (30) (Fig. 3A). Following a high-throughput antiaging drug screening, we identified six compounds that significantly reduced SA- β -Gal activity from two libraries: the Bioactive Compound Library (L2000-Z481077, Selleck, TX) and the FDA-Approved Drug Library (HY-L022,

MCE, NJ) (*SI Appendix*, Fig. S7). Among them, three are known antiaging drugs, including aspirin, metformin, and niacin (50–52), while the other three are undescribed candidates. Notably, sapanisertib was identified as the most effective compound in ameliorating cellular senescence in the intestine of *wrn*^{KO} mutants, as indicated by the inhibition of SA- β -Gal activity (Fig. 3B and *SI Appendix*, Fig. S7). Sapanisertib treatment also reduced the expression levels of *p21* and *p53* (Fig. 3C and D). Furthermore, we observed that the *wrn*^{KO} mutant exhibited a notable reduction

of lifespan, which was subsequently ameliorated by treatment with sapanisertib (Fig. 3E). Swimming activity, a primary indicator of healthspan in zebrafish, showed a significant decline in *wrn*^{KO} mutants at 15 dpf. However, this decline was effectively restored upon treatment with sapanisertib, suggesting the potential of sapanisertib to extend the healthspan of *wrn*^{KO} mutants (Fig. 3F and Movie S1). Additionally, ORO staining assay and WISH result of *cetp* revealed that sapanisertib attenuated the fatty liver phenotype in *wrn*^{KO} mutants (Fig. 3G). DNA damage is one of the major

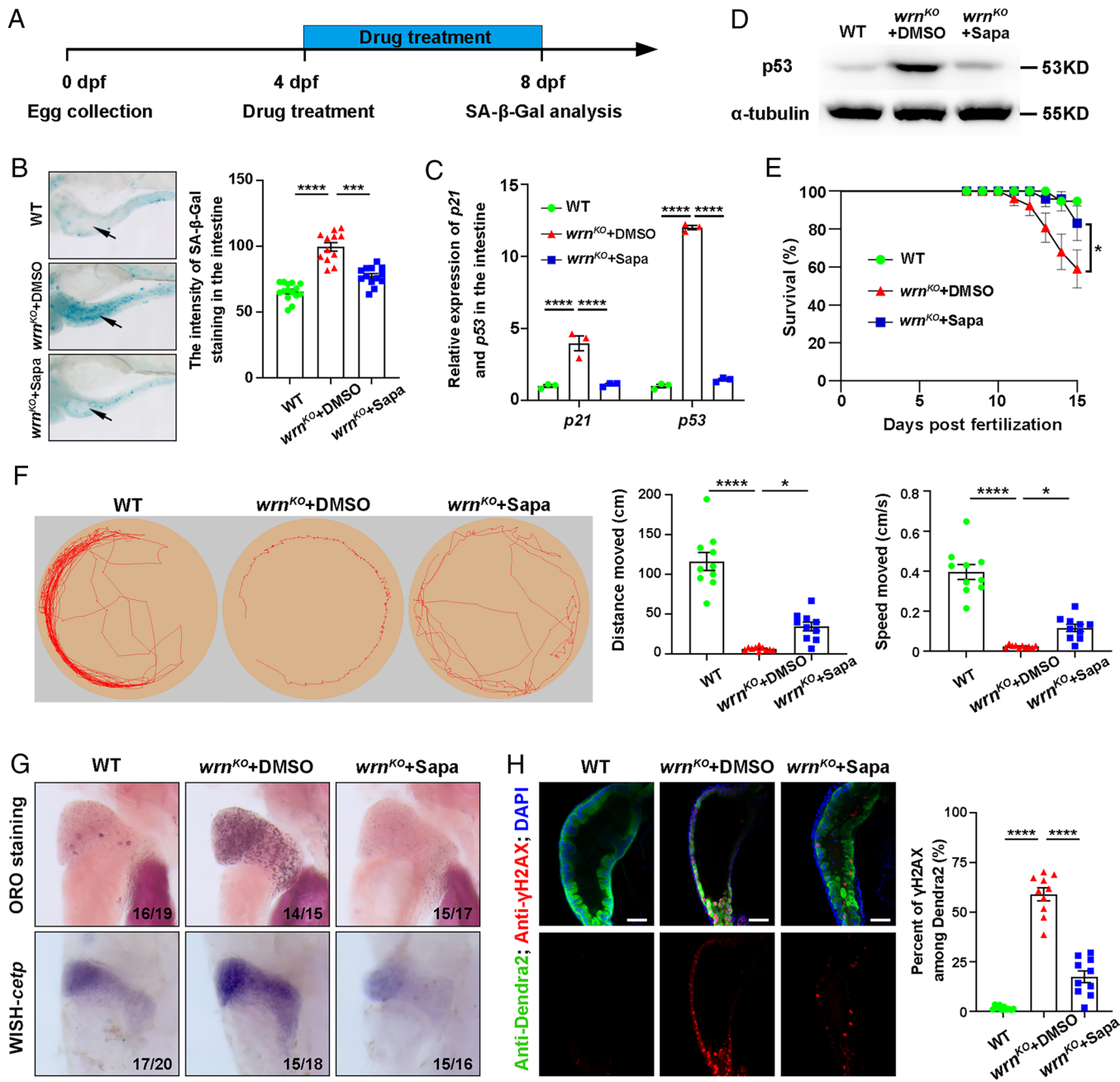


Fig. 3. Drug screening identified that sapanisertib alleviated aging phenotypes in *wrn*^{KO} mutants. (A) Schematic illustration of antiaging drug screening on the zebrafish *wrn*^{KO} mutant. (B) Representative image of SA- β -Gal staining and quantification of the intensity of SA- β -Gal staining in the intestine at 8 dpf ($n = 12$ to 15 for each group). Arrows indicate the intestine region. (C) qPCR analysis of age-related gene expression (*p21* and *p53*) in intestinal samples at 8 dpf ($n = 40$ for each group). (D) Western blot images of *p53* in WT, *wrn*^{KO+DMSO}, and *wrn*^{KO+Sapa} groups in intestinal samples at 8 dpf ($n = 40$ for each group). (E) The percent of survival of the WT ($n = 19$), *wrn*^{KO+DMSO} ($n = 24$), and *wrn*^{KO+Sapa} ($n = 18$) groups from 0 dpf to 15 dpf is presented. (F) Representative swimming tracks (Left) and quantification of total distance traveled and swimming speed (Right) among WT, *wrn*^{KO+DMSO}, and *wrn*^{KO+Sapa} groups at 15 dpf ($n = 10$ for each group). The yellow circle represents the recording field, and the red line represents the swimming track. (G) ORO staining and WISH of *cetp* at 8 dpf. Numbers indicate the proportion of larvae exhibiting the expression shown. (H) Single-optical section images showing the expression of γ H2AX (red), Dendra2 (green), and DAPI (blue) in the intestine of *Tg(fabp2:Dendra2-NTR)* at 8 dpf. Quantification of the percent of γ H2AX ($n = 10$ for each group). (Scale bar, 50 μ m.) Data are presented as mean \pm SEM. Significance was determined by one-way ANOVA, and the survival rate was analyzed with the log-rank test. * $P < 0.05$; ** $P < 0.01$; *** $P < 0.001$; **** $P < 0.0001$. Sapa, sapanisertib.

causes of aging and reducing DNA damage is regarded as a key strategy for delaying aging (43), and we observed that sapanisertib administration reduced DNA damage accumulation significantly in the intestine of the *wrn*^{KO} mutant, as indicated by decreased levels of γH2AX (Fig. 3*H*). However, sapanisertib failed to restore the loss of H3K9me3 in the intestine of *wrn*^{KO} mutants (*SI Appendix*, Fig. S8). Taken together, our data suggest that sapanisertib attenuated most of the accelerated aging phenotypes in *wrn*^{KO} mutant larvae.

Sapanisertib May Attenuate the Aging Phenotypes of the *wrn*^{KO} Mutant by Inhibiting mTORC1/2 Signaling. Genetic and pharmacological evidence indicates that hyperactivation of mTORC1 signaling results in accelerated aging (53, 54). To evaluate the activity of mTORC1 signaling, we analyzed the level of p-S6 and p-4EBP, two well-established downstream effectors of mTORC1 signaling (55). Although p-S6 and p-4EBP were only weakly expressed in WT, their expression was significantly up-regulated in the intestine of *wrn*^{KO} mutants at 8 dpf (Fig. 4 *A–D*), suggesting that hyperactivation of mTORC1 signaling contributed to premature aging in *wrn*^{KO} mutants. However, a significant decrease of mTORC1 signaling was observed in the intestine of *wrn*^{KO} mutants following treatment with sapanisertib (Fig. 4 *A–D*), implying that sapanisertib alleviates the aging phenotype of the *wrn*^{KO} mutant by inhibiting the mTORC1 pathway. Currently, rapamycin is regarded as one of the most promising antiaging drugs, also exerting its antiaging effects through the inhibition of mTORC1 signaling (56). Thus, we conducted a comparative analysis of the antiaging efficacy between sapanisertib and rapamycin, revealing that sapanisertib exhibited a superior effect in ameliorating cellular senescence compared to rapamycin in *wrn*^{KO} mutants (Fig. 4 *E* and *F*). As sapanisertib is a mTORC1/2 dual inhibitor (57), we speculate that sapanisertib ameliorates the aging phenotype of *wrn*^{KO} mutants by inhibiting mTORC1/2 signaling. To assess the activation of mTORC2 signaling, we examined the phosphorylation of Akt at the Ser 473 site (p-Akt S473), a major downstream target of mTORC2 (58). While p-Akt was minimally expressed in WT, its expression was significantly up-regulated in the intestine of *wrn*^{KO} mutants (Fig. 4*G*), indicating hyperactivation of mTORC2 signaling in *wrn*^{KO} mutants. After treatment with sapanisertib, a marked reduction in mTORC2 signaling was observed in the intestine of *wrn*^{KO} mutants, whereas rapamycin had no effect on mTORC2 signaling (Fig. 4*G*). Overall, these results suggest that sapanisertib may attenuate the aging phenotypes of the *wrn*^{KO} mutant by inhibiting both mTORC1 and mTORC2 pathway, which are hyperactivated in *wrn*^{KO} mutants.

To better understand the mechanism of sapanisertib, we treated *wrn*^{KO} mutants with the mTORC2-selective inhibitor JR-AB2-011 (59) and observed a marked reduction of p-Akt levels in the intestine of *wrn*^{KO} mutants, confirming that JR-AB2-011 effectively inhibits mTORC2 signaling (*SI Appendix*, Fig. S9 *D* and *E*). Subsequently, we compared the antiaging efficacy of four treatment groups: sapanisertib, rapamycin, JR-AB2-011, and a combination of rapamycin and JR-AB2-011. Our results showed that the antiaging effect of combined treatment with JR-AB2-011 and rapamycin was comparable to sapanisertib but superior to either rapamycin or JR-AB2-011 alone (*SI Appendix*, Fig. S9 *A–C*). These findings provide further support for the hypothesis that the antiaging effects of sapanisertib are mediated through its dual inhibition of both mTORC1 and mTORC2.

Sapanisertib Alleviated Aging Phenotypes in Both Physiological-Aging Zebrafish and Replicative-Senescence Human Foreskin Fibroblasts (HFF). To further investigate the geroprotective effects of sapanisertib in chronological aging, we analyzed the intestine and kidney marrow of aged WT zebrafish treated with

sapanisertib. Compared with young zebrafish (6-mo-old), aged zebrafish (3-y-old) exhibited significant SA-β-Gal activity in both the intestine and kidney marrow, which was ameliorated by sapanisertib treatment (Fig. 5 *A–C* and *E*). Similarly, sapanisertib treatment increased the proliferative capacity of the intestine and kidney marrow in aged zebrafish (Fig. 5 *A, B, D*, and *F*).

To determine whether the observed increase in cell proliferation improves intestinal barrier function, we performed the Smurf assay, which evaluates gut permeability by detecting the extraluminal accumulation of Blue Dye #1, an indicator of compromised intestinal integrity (60). The results showed significantly higher dye leakage in aged zebrafish compared to young fish (*SI Appendix*, Fig. S10*A*). However, sapanisertib treatment significantly reduced dye leakage in aged zebrafish (*SI Appendix*, Fig. S10*A*), suggesting that increased cell proliferation contributes to improve intestinal barrier function. Additionally, we examined the potential impact of sapanisertib on kidney function by analyzing lymphoid and myeloid cell populations using Wright-Giemsa staining (61). The analysis revealed no significant differences in lymphoid/myeloid ratios between the sapanisertib-treated and DMSO control groups, indicating that sapanisertib fails to improve kidney function in aged zebrafish (*SI Appendix*, Fig. S10*B*).

To evaluate the potential risk of increased cell proliferation leading to spontaneous tumor formation, we performed hematoxylin and eosin staining, a widely used method for evaluating tissue architecture and identifying hallmarks of tumor development (62, 63). The analysis revealed well-preserved villi, organized cellular arrangements, and no signs of nuclear atypia, structural disruption, or invasive growth in the sapanisertib-treated group (*SI Appendix*, Fig. S11*A*). Furthermore, we examined the expression of tumor-related genes (*cdb1*, *cyclinD1*, *cyclinE1*, *twist1*, and *itga5*), which regulate cell adhesion, migration, invasion, and metastasis and are closely linked to tumor progression (64–68). Quantitative PCR analysis demonstrated no significant differences in the expression of these genes between the sapanisertib-treated and DMSO control groups (*SI Appendix*, Fig. S11*B*). Together, these results indicate that sapanisertib treatment does not increase the risk of spontaneous tumor formation or progression in zebrafish tissues.

To explore sapanisertib's impact beyond zebrafish, we investigated its ability to ameliorate senescent phenotypes in replicative-senescence HFF, a well-established model for investigating cellular senescence. An increased SA-β-Gal staining was observed in HFF cells at passage 30, which was attenuated by sapanisertib treatment (Fig. 5 *G* and *H*). Furthermore, sapanisertib treatment increased the cell proliferation rate of HFF cells at passage 30 (Fig. 5 *G* and *I*). Additionally, the lifespan and total cumulative population doublings were extended in sapanisertib-treated HFF cells (Fig. 5*J*). Taken together, these results suggest that in addition to the zebrafish *wrn*^{KO} mutant, sapanisertib also exerts geroprotective effects against chronological aging in WT zebrafish and replicative senescence in HFF cells.

Sapanisertib Alleviated DNA Damage and Maintained Telomere Stability in Both Physiologically Aged Zebrafish and Replicative-Senescence HFF Cells via mTORC1 Inhibition. Since sapanisertib may attenuate the aging phenotypes in *wrn*^{KO} mutants by inhibiting the mTORC1/2 pathway (Fig. 4 and *SI Appendix*, Fig. S9), we hypothesized that sapanisertib also alleviates aging through mTOR signaling in physiologically senescent zebrafish and replicative-senescence HFF cells. Given that increased DNA damage and telomere shortening are hallmarks of aging in zebrafish and human, associated with cellular senescence and functional decline (2, 33, 48), we examined whether sapanisertib mitigates these aging hallmarks. The results of γH2AX staining showed that sapanisertib administration reduced DNA damage

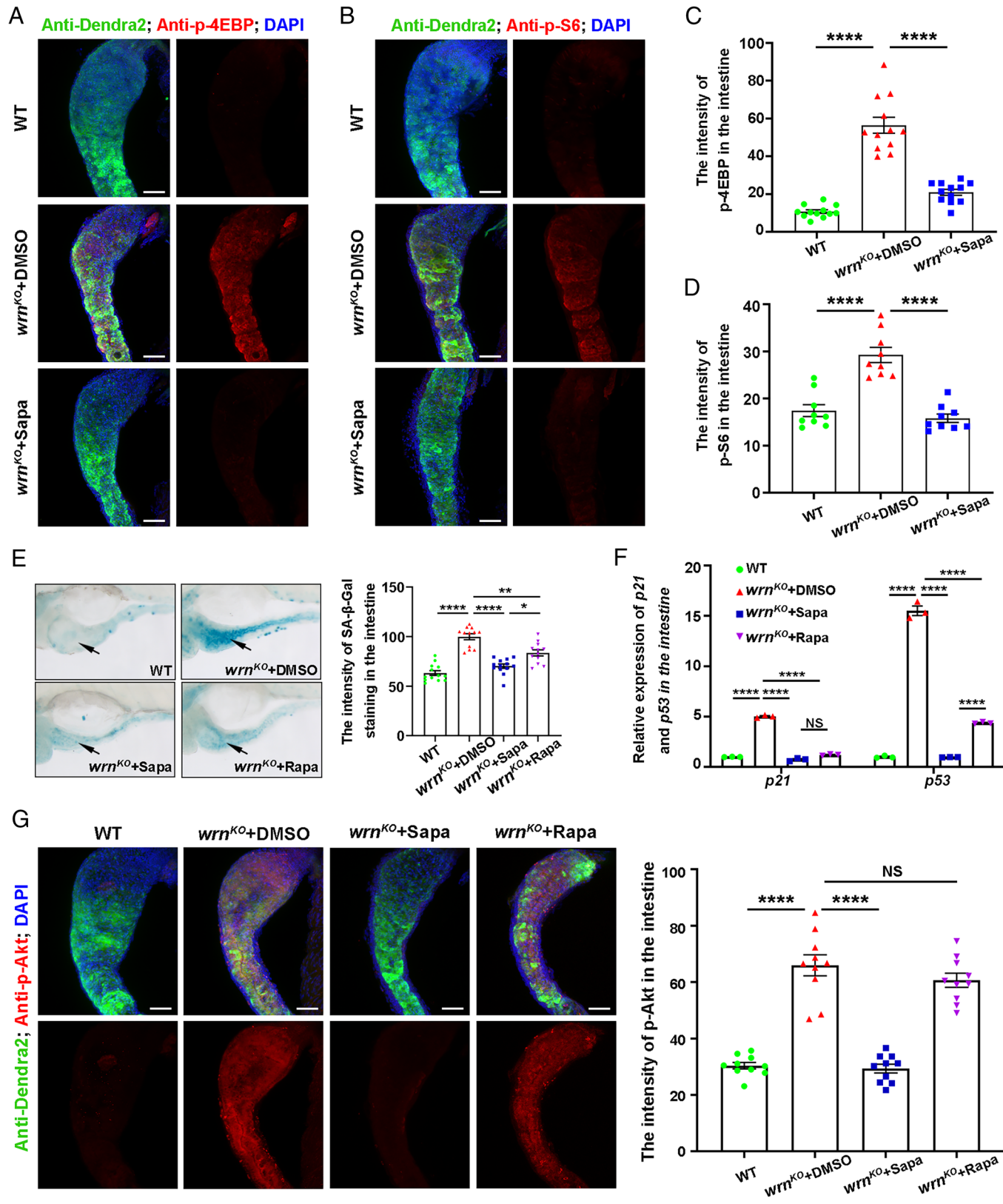


Fig. 4. Sapanisertib may attenuate the aging phenotypes of the *wrn*^{KO} mutant by inhibiting mTORC1/2 signaling. (A–D) Confocal projection images showing the expression of p-4EBP (A, red), p-S6 (B, red), Dendra2 (green), and DAPI (blue) in the intestine of *Tg(fabp2:Dendra2-NTR)* among WT, *wrn*^{KO} + DMSO, and *wrn*^{KO} + Sapa groups at 8dpf. Quantification of the intensity of p-4EBP (C, n = 12 for each group) and p-S6 (D, n = 9 for each group). (E) Representative image of SA-β-Gal staining and quantification of the intensity of SA-β-Gal staining in the intestine at 8 dpf (n = 11 to 14 for each group). Arrows indicate the intestine region. (F) qPCR analysis of age-related gene expression (*p21* and *p53*) in intestinal samples at 8 dpf (n = 40 for each group). (G) Confocal projection images showing the expression of p-Akt (red), Dendra2 (green), and DAPI (blue) in the intestine of *Tg(fabp2:Dendra2-NTR)* among WT, *wrn*^{KO}+DMSO, *wrn*^{KO}+Sapa, and *wrn*^{KO}+Rapa groups at 8dpf. Quantification of the intensity of p-Akt (n = 10 for each group). (Scale bar, 50 μ m.) Data are presented as mean \pm SEM. Significance was determined by one-way ANOVA. NS, not significant; *P < 0.05; **P < 0.01; ***P < 0.0001. Rapa, rapamycin.

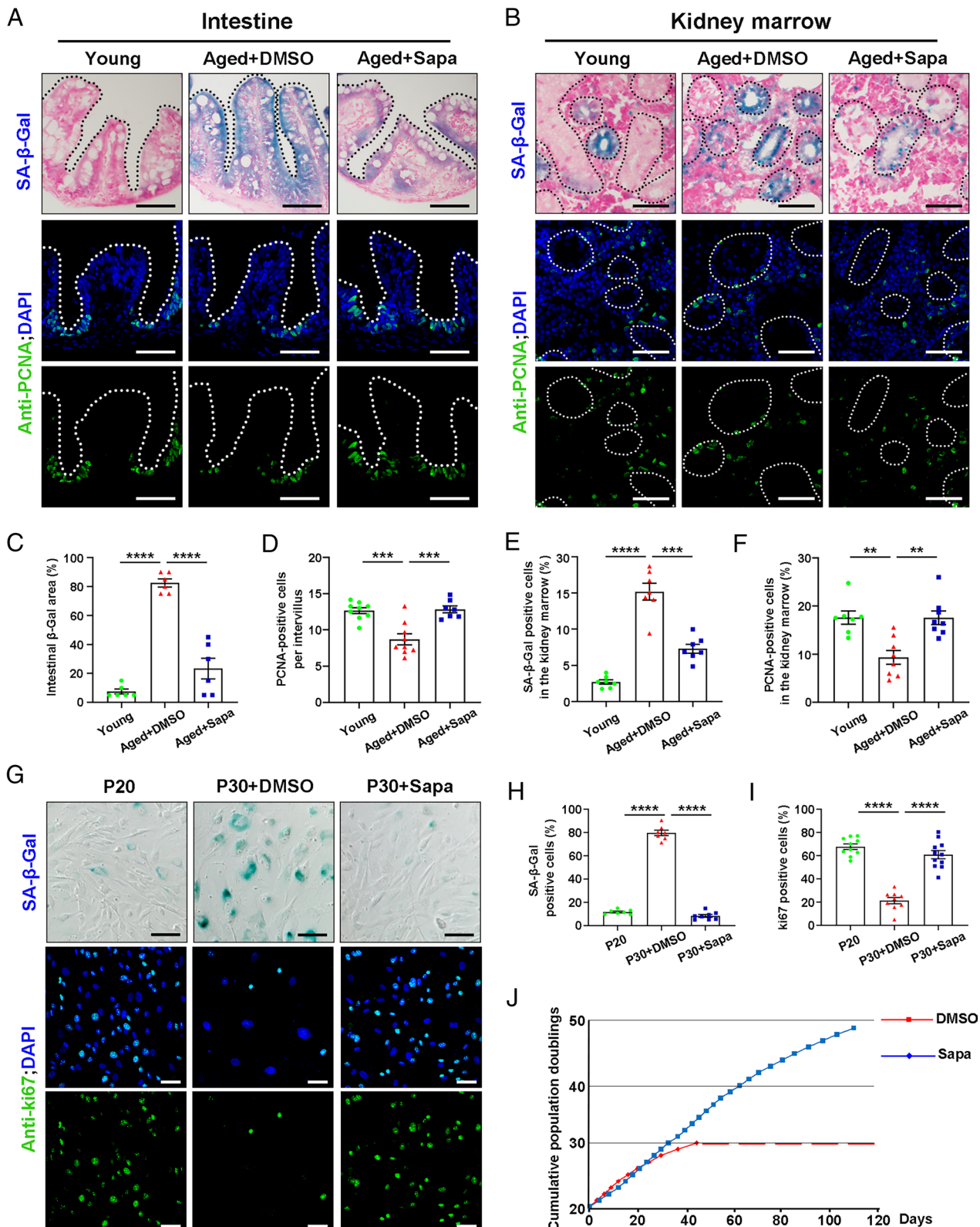


Fig. 5. Sapanisertib alleviated aging phenotypes in both physiological-aging zebrafish and replicative-senescent HFF. (A and B) Representative images of SA- β -Gal staining (Top) and immunofluorescence sections images of proliferation staining (PCNA, Bottom) in the intestine (A) and kidney marrow (B) of young, aged+DMSO, and aged+Sapa groups. (C–F) Quantification of the percent of SA- β -Gal positive area in the intestine (C, $n = 6$ for each group) and kidney marrow (E, $n = 7$ for each group). Quantification of the PCNA-positive cells per intervillus in the intestine (D, $n = 7$ to 9 for each group) and the percent of PCNA-positive cells among kidney marrow (F, $n = 7$ to 8 for each group). (G) Representative image of SA- β -Gal staining and immunofluorescence images of proliferation staining (ki67) in HFF cells of P20, P30+DMSO, and P30+Sapa groups. (H and I) Quantification of the percent of SA- β -Gal staining positive cells (H, $n = 7$ to 8 for each group) and the percent of ki67 positive cells (I, $n = 9$ to 11 for each group) in HFF cells. (J) The total cumulative population doublings of HFF cells in standard conditions (DMSO) and in sapanisertib treatment are depicted. Each dot denotes a passage, and the dashed line indicates the cessation of cell expansion. (Scale bar, 100 μ m.) Data are presented as mean \pm SEM. Significance was determined by one-way ANOVA. ** $P < 0.01$; *** $P < 0.001$; **** $P < 0.0001$. HFF, human foreskin fibroblasts; PCNA, proliferation cell nuclear antigen; P20, passage 20.

accumulation in the intestine of aged zebrafish (Fig. 6 A and C) and replicative-senescent HFF cells (Fig. 6 B and E). Additionally, results of quantitative fluorescence *in situ* hybridization showed that sapanisertib treatment led to a visible but modest increase in telomere fluorescence in aged zebrafish intestines (Fig. 6 A and D), while a significant increase was observed in HFF cells (Fig. 6 B and F), reflecting resistance to age-related telomere attrition. To evaluate the activity of mTOR signaling, we examined the expression of p-4EBP and p-Akt in aged zebrafish and replicative-senescent HFF cells. Sapanisertib administration decreased the activation of mTORC1 signaling in aged zebrafish and HFF cells (Fig. 6 G–J), however, the mTORC2 signaling was not activated in the intestines of aged zebrafish or in replicative-senescent HFF cells (*SI Appendix*, Fig. S12 A–D). These results imply that sapanisertib alleviates the aging phenotype of physiological-aging zebrafish and replicative-senescent HFF by inhibiting the mTORC1 pathway.

Discussion

As global populations are rapidly aging, it is imperative to identify geroprotective drugs that attenuate age-related deterioration of health. Hampered by the long lifespan of vertebrates, the initial screening of antiaging drugs is mainly limited to *in vitro* or invertebrate organisms such as *C. elegans* and *Drosophila* (19). Here, we identified an accelerated aging mutant in zebrafish that recapitulated the age-related characteristics of WS patients, making it suitable for high-throughput screening of antiaging compounds. Furthermore, we found that sapanisertib attenuated the aging phenotypes in the *wrn*^{KO} mutant, HFF cells, and WT aged zebrafish.

Due to a series of premature aging features, WS, a premature aging syndrome closely resembling normal human aging, has been extensively researched in the field of aging and considered a valuable model for studying physiological human aging (26, 27). However, unlike WS patients, *Wrn* knockout mice are phenotypically normal and do not recapitulate the features observed in WS patients (35, 36). Thus, the WS mouse models are not a desirable option in aging research, resulting in most of the mechanistic data of WS being obtained from cell lines derived from WS patients and two invertebrate animal models, *C. elegans* and *Drosophila* (34). A previous study of the *wrn* mutant in zebrafish primarily focused on bone development, observing a shortened body length, which is consistent with the short stature of WS patients. However, aside from this characteristic, the model did not exhibit the broader spectrum of aging-related features observed in human WS patients (28). Similarly, a study on the *blm* mutant, another member of the RECQL helicase family, revealed its role in germ line development and demonstrated a shortened lifespan, which is consistent with aging characteristics. However, this model failed to recapitulate other key premature aging phenotypes such as DNA damage accumulation (29).

In contrast, our *wrn*^{KO} mutant recapitulates key features of WS in the intestine at 8 dpf, such as cellular senescence and genomic instability. Previous studies have shown that the intestine is one of the first organs to exhibit aging markers, including telomere shortening, DNA damage, and the accumulation of senescent cells (31–33), highlighting its potential as an indicator of systemic aging, thus suggesting that *wrn*^{KO} mutants develop a premature aging phenotype. The small size of zebrafish embryos at 8 dpf enables high-throughput drug screening with minimal compound usage, making the *wrn*^{KO} mutant an efficient, cost-effective model for rapid screening of WS therapeutics. Additionally, the *wrn*^{KO} mutant also exhibits several features of human

chronological aging, such as cellular senescence, DNA damage accumulation, and increased inflammation, making it a valuable model for identifying compounds that may also alleviate chronological aging. Indeed, using this model, we identified three known compounds that alleviate chronological aging, highlighting the broader applicability of the *wrn*^{KO} mutant in screening drugs targeting both WS and chronological aging. Furthermore, we identified sapanisertib as a geroprotective agent against both premature and chronological aging. Sapanisertib, as an orally bioavailable and highly selective mTOR kinase inhibitor of mTORC1/2, has an efficient therapeutic effect on various cancers. Sapanisertib has entered phase II clinical trials as an antitumor drug, demonstrating manageable toxicity profiles and suggesting its potential as a promising therapeutic option for treating WS and promoting healthy aging.

In addition, we observed that treatment with sapanisertib exhibited a superior effect in ameliorating cellular senescence compared to rapamycin in zebrafish *wrn*^{KO} mutants. We hypothesize that this discrepancy may be attributed to the dual inhibition of mTORC1 and mTORC2 by sapanisertib, whereas short-term treatment with rapamycin only inhibits mTORC1. Although the role of mTORC1 in aging is relatively well defined, the relationship between mTORC2 and aging is comparatively less studied. Most studies indicate that mTORC2 activity has been positively associated with longevity and healthy aging. It has been reported that depletion of hypothalamic or hepatic *Rictor* decreases lifespan in mice (69, 70). In flies, the overexpression of Rictor extends lifespan (71). By contrast, there may be benefits of inhibiting mTORC2 in certain contexts. It was shown that suppression of mTORC2 ameliorates survival and abnormal behaviors in a *Pten* knockout mouse model (72) and that the mTORC2 substrate Akt1 haploinsufficiency leads to extended lifespan in mice (73). Here, we demonstrated that hyperactivation of mTORC2 may be a significant factor in the premature aging of *wrn*^{KO} mutants, and inhibition of mTORC2 activity alleviated the premature aging phenotypes. Thus, understanding both the positive and negative roles of mTORC2 in premature aging and age-related disease is of great significance in the future.

This study had several limitations. First, while the *wrn*^{KO} mutant exhibits many hallmark features of chronological aging, it remains fundamentally a model of premature aging. Consequently, drugs identified using this model may hold potential as treatments for WS, but their efficacy in delaying chronological aging requires further validation in chronological aging models. Second, although sapanisertib showed significant antiaging effects in zebrafish and human cell line, its long-term safety and efficacy in mammals and humans have not been fully explored, requiring extensive clinical trials to assess potential risks and benefits comprehensively. Additionally, while dual inhibition of mTORC1/2 appears beneficial in this study, the complex roles of mTORC2 in aging and longevity need further elucidation. Third, although the *wrn*^{KO} mutant recapitulates key features of WS, making it an ideal model for studying this syndrome, its premature mortality before sexual maturity, potentially attributed to intestinal barrier dysfunction, limits its relevance for studying later-life stages, since WS patients typically survive into adulthood.

In conclusion, our study revealed that the zebrafish *wrn*^{KO} mutant recapitulated the premature aging characteristics observed in WS patients, providing a valuable model for WS research and screening of geroprotective drugs in vertebrates. Additionally, the present work identified sapanisertib as a geroprotective agent against both premature and chronological aging, supporting the role of sapanisertib as a unique therapeutic option for treating premature aging and promoting healthy aging.

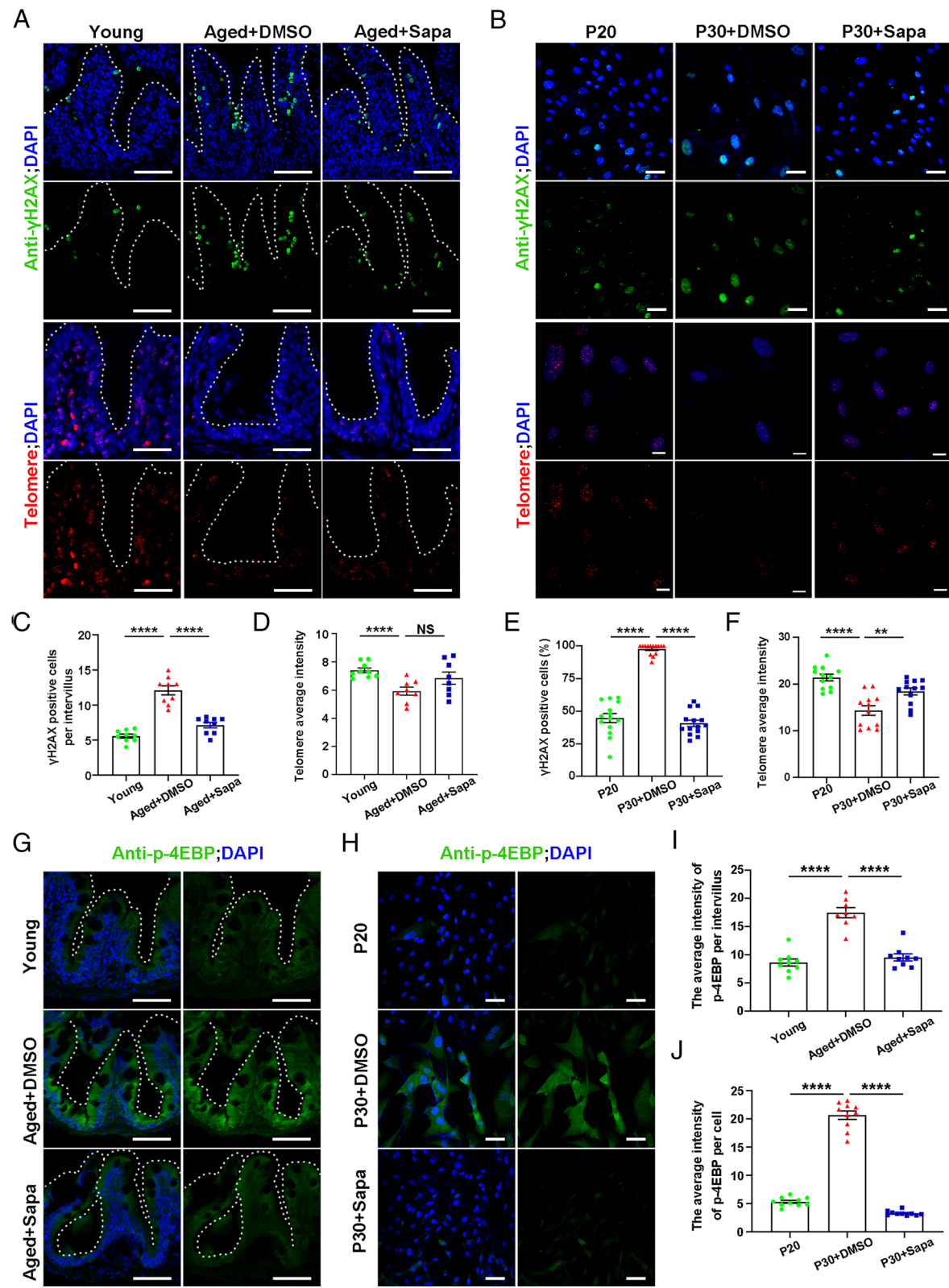


Fig. 6. Sapanisertib attenuated DNA damage and maintained telomeres stability in both physiological-aging zebrafish and replicative-senescent HFF cells via mTORC1 inhibition. (A and B) Representative images of γ H2AX staining (Top) and immunofluorescence section images of telomere staining (Bottom) in the intestine of young, aged+DMSO, and aged+Sapa groups (A) and HFF cells of P20, P30+DMSO, and P30+Sapa groups (B). (C–F) Quantification of the γ H2AX-positive cells per villus in the intestine (C, n = 9 for each group) and in HFF cells (E, n = 14 for each group). Quantification of the intensity of the average fluorescence intensity in the intestine (D, n = 10 for each group) and HFF cells (F, n = 12 for each group). (G–J) Representative images of p-4EBP staining in the intestine (G) and HFF cells (H). Quantification of the intensity of p-4EBP per villus in the intestine (I, n = 8 to 9 for each group) and in HFF cells (J, n = 10 for each group). (Scale bar, 100 μ m.) Data are presented as mean \pm SEM. Significance was determined by one-way ANOVA. NS, not significant; **P < 0.01; ***P < 0.001; ****P < 0.0001. HFF, human foreskin fibroblasts; P20, passage 20.

Materials and Methods

Zebrafish Husbandry and Strains. All animal procedures were performed according to protocols approved by the Institutional Animal Care and Use Committee of Southwest University (Approval No. LAC2023-1-0052) and were consistent with the NIH Guide for the Care and Use of Laboratory Animals. The zebrafish lines AB, *Tg(fabp2:Dendra2-NTR)^{cq161}*, *Tg(hsp70l:wrn-p2A-mCherry)^{cq215}*, *met*^{cq216} mutant, *wrn*^{KO cq217} mutant, *tp53*^{M214K} mutant, and the polymorphic line SJD were used in this study.

Cell Culture and Cell Lines. HFF cells were kindly provided by Cell Bank of Chinese Academy of Sciences. Cells were cultured in Dulbecco's Modified Eagle's Medium (Gibco) with 15% heat-inactivated fetal bovine serum (FBS, Gibco) at 37 °C in a humidified atmosphere of 5% CO₂ and 95% air. The growth medium was further supplemented with 100 U/mL penicillin and 0.1 mg/mL streptomycin to prevent contamination. Subculturing was performed upon reaching confluence using a solution containing 0.25% trypsin and 0.02% EDTA to detach cells from the culture vessel. HFF cells were treated with sapanisertib at concentration of 5 nM starting from passage 20 to investigate its effects on cellular senescence.

ENU Mutagenesis and Screening. ENU (Sigma, USA) mutagenesis was conducted as previously reported (74) for mutations affecting cell senescence. Briefly, adult WT male zebrafish were exposed to ENU (3.5 mM) for 1 h at 5-d intervals and repeated for six cycles. Two weeks after the completion of the final ENU treatment, these males were outcrossed with WT females to generate F1 families. Sexually matured F1 fish were then mated to WT line to generate F2 families, and mature F2 siblings were intercrossed to generate F3 embryos for subsequent screening.

In the ENU mutagenesis screening, we analyzed at least 60 embryos in each experiment to ensure a sample size sufficient for statistical significance. Zebrafish larvae typically consume the supportive yolk by 6 dpf, and without food, their health declines after 9 dpf. To avoid potential spurious effects from caloric restriction or other nutritional deficiencies, we selected 8 dpf as the experimental endpoint. This time point also facilitates high-throughput ENU mutagenesis screening and subsequent drug screening. Additionally, to minimize variability in the SA-β-Gal assay, we included tert-butyl hydroperoxide (BHP)-induced embryonic aging as a positive control and WT embryos as a negative control to enhance the accuracy and reproducibility of the staining results.

Chemical Screening. The screening library comprises a total of 2,442 compounds, including a customized bioactive compound library (L2000-Z481077,

Selleck, TX) and an FDA-approved drug library (HY-L022, MCE, NJ). Six *met* mutant larvae at 4 dpf were aliquoted into each well of a 24-well plate in a total volume of 0.5 mL egg water with a drug concentration of 10 μmol/L. The *met* mutants were treated with either DMSO or water as a negative control and with rapamycin, a well-known antiaging drug, as a positive control. The plates were then incubated for 4 d at 28.5 °C. At 8 dpf, larvae were fixed in 4% PFA at 4 °C overnight and assessment of cellular senescence using SA-β-Gal staining. The antiaging efficacy of each compound was evaluated by comparing SA-β-Gal staining intensity across treatment groups. A reduced signal indicated lower senescence levels and suggested potential antiaging effects. Initial positive hits were retested to confirm reproducibility, with a minimum of three additional independent trials using the same protocol and concentration. Compounds consistently showing significant reductions in SA-β-Gal activity were further evaluated in independent assays to quantify their antiaging efficacy.

Statistical Analyses. All statistical calculations in this study were performed using GraphPad Prism 9.5. Student's *t* test was used for comparisons between two groups, while one-way ANOVA was performed to assess differences among three or more groups. Survival rates were analyzed using the log-rank test. Values of *P* < 0.05 were considered statistically significant (**P* < 0.05; ***P* < 0.01; ****P* < 0.001; *****P* < 0.0001); NS (*P* ≥ 0.05) indicated not significant. All values were presented as mean ± SEM.

Data, Materials, and Software Availability. All study data are included in the article and/or [supporting information](#). The RNA-seq data in this study have been submitted to the National Center for Biotechnology Information (NCBI) Sequence Read Archive (SRA), <https://www.ncbi.nlm.nih.gov/sra> (accession no. PRJNA1186411) (75).

ACKNOWLEDGMENTS. We especially thank Li Li for providing essential technical support for the behavioral assay as well as for the Wright-Giemsa staining. This work was supported by the National Natural Science Foundation of China (32192400 and 32430032), the National Key Research and Development Program of China (2021YFA0805000), Fund of Fudan University and Cao'ejiang Basic Research (24FCB04), and Shanghai Municipal Science and Technology Major Project (2023SHZDZX02A10).

Author affiliations: ^aState Key Laboratory of Genetic Engineering, School of Life Sciences, Liver Cancer Institute of Zhongshan Hospital, Fudan University, Shanghai 200438, China; and ^bInstitute of Developmental Biology and Regenerative Medicine, Southwest University, Chongqing 400715, China

1. L. Pio-Lopez, M. Levin, Aging as a loss of morphostatic information: A developmental bioelectricity perspective. *Ageing Res. Rev.* **97**, 102310 (2024).
2. C. Lopez-Otin, M. A. Blasco, I. Partridge, M. Serrano, G. Kroemer, Hallmarks of aging: An expanding universe. *Cell* **186**, 243–278 (2023).
3. L. Harkema, S. A. Youssef, A. de Bruin, Pathology of mouse models of accelerated aging. *Vet. Pathol.* **53**, 366–389 (2016).
4. L. Guarente, C. Kenyon, Genetic pathways that regulate ageing in model organisms. *Nature* **408**, 255–262 (2000).
5. M. D. W. Piper, L. Partridge, *Drosophila* as a model for ageing. *Biochim. Biophys. Acta Mol. Basis Dis.* **1864**, 2707–2717 (2018).
6. A. Brunet, Old and new models for the study of human ageing. *Nat. Rev. Mol. Cell Biol.* **21**, 491–493 (2020).
7. J. Campisi *et al.*, From discoveries in ageing research to therapeutics for healthy ageing. *Nature* **571**, 183–192 (2019).
8. E. T. Keller, J. M. Murtha, The use of mature zebrafish (*Danio rerio*) as a model for human aging and disease. *Comp. Biochem. Physiol. C Toxicol. Pharmacol.* **138**, 335–341 (2004).
9. S. Chaib, T. Tcheknoria, J. L. Kirkland, Cellular senescence and senolytics: The path to the clinic. *Nat. Med.* **28**, 1556–1568 (2022).
10. N. Cai, Y. Wu, Y. Huang, Induction of accelerated aging in a mouse model. *Cells* **11**, 1418 (2022).
11. M. S. Abou-Daheche, F. E. Williams, Aging, age-related diseases, and the zebrafish model. *J. Dement. Alzheimer's Dis.* **1**, 48–71 (2024).
12. L. G. Fong *et al.*, A protein farnesyltransferase inhibitor ameliorates disease in a mouse model of progeria. *Science* **311**, 1621–1623 (2006).
13. B. Novoa *et al.*, Rag1 immunodeficiency-induced early aging and senescence in zebrafish are dependent on chronic inflammation and oxidative stress. *Aging Cell* **18**, e13020 (2019).
14. Y. Kim, H. G. Nam, D. R. Valenzano, The short-lived African turquoise killifish: An emerging experimental model for ageing. *Dis. Model. Mech.* **9**, 115–129 (2016).
15. J. Van Houcke *et al.*, A short dasatinib and quercetin treatment is sufficient to reinstate potent adult neurogenesis in the aged killifish. *NPJ Regen. Med.* **8**, 31 (2023).
16. R. Strong *et al.*, Lifespan benefits for the combination of rapamycin plus acarbose and for captopril in genetically heterogeneous mice. *Aging Cell* **21**, e13724 (2022).
17. R. Strong *et al.*, Evaluation of resveratrol, green tea extract, curcumin, oxaloacetic acid, and medium-chain triglyceride oil on life span of genetically heterogeneous mice. *J. Gerontol. A Biol. Sci. Med. Sci.* **68**, 6–16 (2013).
18. A. Brunet, Old and new models for the study of human ageing. *Nat. Rev. Mol. Cell Biol.* **21**, 491–493 (2020), 10.1038/s41580-020-0266-4.
19. J. Folch *et al.*, Experimental models for aging and their potential for novel drug discovery. *Curr. Neuropharmacol.* **16**, 1466–1483 (2018).
20. K. Howe *et al.*, The zebrafish reference genome sequence and its relationship to the human genome. *Nature* **496**, 498–503 (2013).
21. M. J. Casey, R. A. Stewart, Pediatric cancer models in zebrafish. *Trends Cancer* **6**, 407–418 (2020).
22. J. M. González-Rosa, Zebrafish models of cardiac disease: From fortuitous mutants to precision medicine. *Circ. Res.* **130**, 1803–1826 (2022).
23. D. C. Pant, T. V. Nazarko, Selective autophagy: The rise of the zebrafish model. *Autophagy* **17**, 3297–3305 (2021).
24. E. E. Patton, L. I. Zon, D. M. Langenau, Zebrafish disease models in drug discovery: From preclinical modelling to clinical trials. *Nat. Rev. Drug Discov.* **20**, 611–628 (2021).
25. C. A. MacRae, R. T. Peterson, Zebrafish as a mainstream model for in vivo systems pharmacology and toxicology. *Annu. Rev. Pharmacol. Toxicol.* **63**, 43–64 (2023).
26. J. Oshima, J. M. Sidorova, R. J. Monnat, Werner syndrome: Clinical features, pathogenesis and potential therapeutic interventions. *Ageing Res. Rev.* **33**, 105–114 (2017).
27. R. A. Shamanna, D. L. Croteau, J.-H. Lee, V. A. Bohr, Recent advances in understanding werner syndrome. *F1000Research* **6**, 1779 (2017).
28. Y. Tian *et al.*, WRN promotes bone development and growth by unwinding SHOX-G-quadruplexes via its helicase activity in Werner syndrome. *Nat. Commun.* **13**, 5456 (2022).
29. T. Annus *et al.*, Bloom syndrome helicase contributes to germ line development and longevity in zebrafish. *Cell Death Dis.* **13**, 363 (2022).
30. G. P. Dimri *et al.*, A biomarker that identifies senescent human cells in culture and in aging skin *in vivo*. *Proc. Natl. Acad. Sci. U.S.A.* **92**, 9363–9367 (1995).
31. M. El Maï *et al.*, Gut-specific telomerase expression counteracts systemic aging in telomerase-deficient zebrafish. *Nat. Aging* **3**, 567–584 (2023).

32. M. El Mai, M. Marzullo, I. P. de Castro, M. G. Ferreira, Opposing p53 and mTOR/AKT promote an in vivo switch from apoptosis to senescence upon telomere shortening in zebrafish. *Elife* **9**, e54935 (2020).
33. L. Harrington *et al.*, Short telomeres in key tissues initiate local and systemic aging in zebrafish. *PLoS Genet.* **12**, e1005798 (2016).
34. S. Lautrup *et al.*, Studying Werner syndrome to elucidate mechanisms and therapeutics of human aging and age-related diseases. *Biogerontology* **20**, 255–269 (2019). 10.1007/s10522-019-09798-2.
35. M. Lebel, P. Leder, A deletion within the murine Werner syndrome helicase induces sensitivity to inhibitor of topoisomerase and loss of cellular proliferative capacity. *Proc. Natl. Acad. Sci. U.S.A.* **95**, 13097–13102 (1998).
36. D. B. Lombard *et al.*, Mutations in the WRN gene in mice accelerate mortality in a p53-null background. *Mol. Cell Biol.* **20**, 3286–3291 (2000).
37. S. Chang *et al.*, Essential role of limiting telomeres in the pathogenesis of Werner syndrome. *Nat. Genet.* **36**, 877–882 (2004).
38. E. Sikora, A. Bielak-Zmijewska, G. Mosieniak, A common signature of cellular senescence; does it exist? *Ageing Res. Rev.* **71**, 101458 (2021).
39. R. Kulikov *et al.*, Mdm2 facilitates the association of p53 with the proteasome. *Proc. Natl. Acad. Sci. U.S.A.* **107**, 10038–10043 (2010).
40. K. Tsukamoto *et al.*, Management guideline for Werner syndrome 2020 1. Dyslipidemia and fatty liver associated with Werner syndrome. *Geriatr. Gerontol. Int.* **21**, 133–138 (2021).
41. J. Oshima, J. M. Sidorova, R. J. Monnat Jr., Werner syndrome: Clinical features, pathogenesis and potential therapeutic interventions. *Ageing Res. Rev.* **33**, 105–114 (2017).
42. K. Ariyoshi, K. Suzuki, M. Goto, M. Watanabe, S. Kodama, Increased chromosome instability and accumulation of DNA double-strand breaks in Werner syndrome cells. *J. Radiat. Res.* **48**, 219–231 (2007).
43. B. Schumacher, J. Pothof, J. Vijg, J. H. J. Hoeijmakers, The central role of DNA damage in the ageing process. *Nature* **592**, 695–703 (2021).
44. X. Wei *et al.*, Extensive jejunal injury is repaired by migration and transdifferentiation of ileal enterocytes in zebrafish. *Cell Rep.* **42**, 112660 (2023).
45. W. Zhang *et al.*, Aging stem cells. A Werner syndrome stem cell model unveils heterochromatin alterations as a driver of human aging. *Science* **348**, 1160–1163 (2015).
46. S. Bergmann *et al.*, tp53 mutant zebrafish develop malignant peripheral nerve sheath tumors. *Proc. Natl. Acad. Sci. U.S.A.* **102**, 407–412 (2005).
47. M. Rera, R. I. Clark, D. W. Walker, Intestinal barrier dysfunction links metabolic and inflammatory markers of aging to death in Drosophila. *Proc. Natl. Acad. Sci. U.S.A.* **109**, 21528–21533 (2012).
48. C. Aging Biomarker *et al.*, Biomarkers of aging. *Sci. China Life Sci.* **66**, 893–1066 (2023).
49. L. Zhang *et al.*, Improving intestinal inflamming to delay aging? A new perspective. *Mech. Ageing Dev.* **214**, 111841 (2023).
50. L. Guarente, D. A. Sinclair, G. Kroemer, Human trials exploring anti-aging medicines. *Cell Metab.* **36**, 354–376 (2024).
51. Y. Yang *et al.*, Metformin decelerates aging clock in male monkeys. *Cell* **187**, 6358–6378.e29 (2024).
52. J. J. McNeil *et al.*, Effect of aspirin on cardiovascular events and bleeding in the healthy elderly. *N. Engl. J. Med.* **379**, 1509–1518 (2018).
53. G. Y. Liu, D. M. Sabatini, mTOR at the nexus of nutrition, growth, ageing and disease. *Nat. Rev. Mol. Cell Biol.* **21**, 183–203 (2020).
54. T. Weichhart, mTOR as regulator of lifespan, aging, and cellular senescence: A mini-review. *Gerontology* **64**, 127–134 (2018).
55. R. A. Saxton, D. M. Sabatini, mTOR signaling in growth, metabolism, and disease. *Cell* **168**, 960–976 (2017).
56. J. B. Mannick, D. W. Lamming, Targeting the biology of aging with mTOR inhibitors. *Nat. Aging* **3**, 642–660 (2023).
57. L. B. Arendse *et al.*, The anticancer human mTOR inhibitor sapanisertib potently inhibits multiple Plasmid kinases and life cycle stages. *Sci. Transl. Med.* **14**, eab07219 (2022).
58. Y. Wang *et al.*, The kinase complex mTORC2 promotes the longevity of virus-specific memory CD4+ T cells by preventing ferroptosis. *Nat. Immunol.* **23**, 303–317 (2022).
59. D. Li *et al.*, SLAMF3 and SLAMF4 are immune checkpoints that constrain macrophage phagocytosis of hematopoietic tumors. *Sci. Immunol.* **7**, eabj5501 (2022).
60. R. R. Martins, A. W. McCracken, M. J. P. Simons, C. M. Henriques, M. Rera, How to catch a Smurf? Ageing and beyond... In vivo assessment of intestinal permeability in multiple model organisms. *Bio Protoc.* **8**, e2722 (2018).
61. D. Traver *et al.*, Transplantation and in vivo imaging of multilineage engraftment in zebrafish bloodless mutants. *Nat. Immunol.* **4**, 1238–1246 (2003).
62. J. W. Lu, D. Raghuram, P. A. Fong, Z. Gong, Inducible intestine-specific expression of kras(V12) triggers intestinal tumorigenesis in transgenic zebrafish. *Neoplasia* **20**, 1187–1197 (2018).
63. N. Kochetkov *et al.*, Ability of *Lactobacillus brevis* 47f to alleviate the toxic effects of imidacloprid low concentration on the histological parameters and cytokine profile of zebrafish (*Danio rerio*). *Int. J. Mol. Sci.* **24**, 12290 (2023).
64. T. Ye *et al.*, Cdh1 functions as an oncogene by inducing self-renewal of lung cancer stem-like cells via oncogenic pathways. *Int. J. Biol. Sci.* **16**, 447–459 (2020).
65. H. Samarendra *et al.*, A meta-analysis of CXCL12 expression for cancer prognosis. *Br. J. Cancer* **117**, 124–135 (2017).
66. J. A. Burger, T. J. Kipps, CXCR4: A key receptor in the crosstalk between tumor cells and their microenvironment. *Blood* **107**, 1761–1767 (2006).
67. Q. Qin, Y. Xu, T. He, C. Qin, J. Xu, Normal and disease-related biological functions of Twist1 and underlying molecular mechanisms. *Cell Res.* **22**, 90–106 (2012).
68. C. Zhang *et al.*, ZNF460-mediated circRPPH1 promotes TNBC progression through ITGA5-induced FAK/PI3K/AKT activation in a ceRNA manner. *Mol. Cancer* **23**, 33 (2024).
69. K. Chellappa *et al.*, Hypothalamic mTORC2 is essential for metabolic health and longevity. *Aging Cell* **18**, e13014 (2019).
70. S. I. Arriola Apelo *et al.*, Ovariectomy uncouples lifespan from metabolic health and reveals a sex-hormone-dependent role of hepatic mTORC2 in aging. *Elife* **9**, e56177 (2020).
71. K. Chang *et al.*, TGFβ-INHB/activin signaling regulates age-dependent autophagy and cardiac health through inhibition of MTORC2. *Autophagy* **16**, 1807–1822 (2020).
72. C. J. Chen *et al.*, Therapeutic inhibition of mTORC2 rescues the behavioral and neurophysiological abnormalities associated with Pten-deficiency. *Nat. Med.* **25**, 1684–1690 (2019).
73. A. Nojima *et al.*, Haplousufficiency of akt1 prolongs the lifespan of mice. *PLoS One* **8**, e69178 (2013).
74. L. Solnica-Krezel, A. F. Schier, W. Driever, Efficient recovery of ENU-induced mutations from the zebrafish germline. *Genetics* **136**, 1401–1420 (1994).
75. J. Ma *et al.*, Establishment and application of a zebrafish model of Werner Syndrome identifies sapanisertib as a potential antiaging drug. NCBI SRA. <https://www.ncbi.nlm.nih.gov/sra/?term=PRJNA1186411>. Deposited 15 November 2024.